

CERN-EP-2016-323

December 28, 2016

Revised version:

October 1, 2018

Measurement of the π^0 Electromagnetic Transition Form Factor Slope

The NA62 collaboration *

Abstract

The NA62 experiment collected a large sample of charged kaon decays in 2007 with a highly efficient trigger for decays into electrons. A measurement of the π^0 electromagnetic transition form factor slope parameter from 1.11×10^6 fully reconstructed $K^\pm \rightarrow \pi^\pm \pi_D^0$, $\pi_D^0 \rightarrow e^+ e^- \gamma$ events is reported. The measured value $a = (3.68 \pm 0.57) \times 10^{-2}$ is in good agreement with theoretical expectations and previous measurements, and represents the most precise experimental determination of the slope in the time-like momentum transfer region.

Accepted for publication in Physics Letters B

*contact: michal.koval@cern.ch, nicolas.lurkin@cern.ch

The NA62 collaboration

C. Lazzeroni¹, N. Lurkin^{*,2}, A. Romano

University of Birmingham, Edgbaston, Birmingham, B15 2TT, United Kingdom

T. Blazek, M. Koval^{*,3}

*Faculty of Mathematics, Physics and Informatics, Comenius University in Bratislava,
842 48 Bratislava, Slovakia*

A. Ceccucci, H. Danielsson, V. Falaleev, L. Gatignon, S. Goy Lopez⁴,

B. Hallgren⁵, A. Maier, A. Peters, M. Piccini⁶, P. Riedler

CERN, CH-1211 Genève 23, Switzerland

P.L. Frabetti, E. Gersabeck⁷, V. Kekelidze, D. Madigozhin, M. Misheva⁸,
N. Molokanova, S. Movchan, Yu. Potrebenikov, S. Shkarovskiy, A. Zinchenko[†],

Joint Institute for Nuclear Research, 141980 Dubna (MO), Russia

P. Rubin⁹

George Mason University, Fairfax, VA 22030, USA

W. Baldini, A. Cotta Ramusino, P. Dalpiaz, M. Fiorini, A. Gianoli,

A. Norton, F. Petrucci, M. Savrié, H. Wahl

*Dipartimento di Fisica e Scienze della Terra dell'Università e Sezione dell'INFN di Ferrara,
I-44122 Ferrara, Italy*

A. Bizzeti¹⁰, F. Bucci¹¹, E. Iacopini¹¹, M. Lenti, M. Veltri¹²

Sezione dell'INFN di Firenze, I-50019 Sesto Fiorentino, Italy

A. Antonelli, M. Moulson, M. Raggi¹³, T. Spadaro

Laboratori Nazionali di Frascati, I-00044 Frascati, Italy

K. Eppard, M. Hita-Hochgesand, K. Kleinknecht, B. Renk, R. Wanke, A. Winhart⁵

Institut für Physik, Universität Mainz, D-55099 Mainz, Germany¹⁴

R. Winston

University of California, Merced, CA 95344, USA

V. Bolotov[†], V. Duk⁶, E. Gushchin

Institute for Nuclear Research, 117312 Moscow, Russia

F. Ambrosino, D. Di Filippo, P. Massarotti, M. Napolitano, V. Palladino¹⁵, G. Saracino

Dipartimento di Fisica dell'Università e Sezione dell'INFN di Napoli, I-80126 Napoli, Italy

G. Anzivino, E. Imbergamo, R. Piandani¹⁶, A. Sergi⁵

Dipartimento di Fisica dell'Università e Sezione dell'INFN di Perugia, I-06100 Perugia, Italy

P. Cenci, M. Pepe

Sezione dell'INFN di Perugia, I-06100 Perugia, Italy

F. Costantini, N. Doble, S. Giudici, G. Pierazzini[†], M. Sozzi, S. Venditti

Dipartimento di Fisica dell'Università e Sezione dell'INFN di Pisa, I-56100 Pisa, Italy

S. Balev[†], G. Collazuol¹⁷, L. DiLella, S. Gallorini¹⁷, E. Goudzovski^{1,2,5},

G. Lamanna¹⁸, I. Mannelli, G. Ruggiero¹⁹

Scuola Normale Superiore e Sezione dell'INFN di Pisa, I-56100 Pisa, Italy

C. Cerri, R. Fantechi

Sezione dell'INFN di Pisa, I-56100 Pisa, Italy

S. Kholodenko, V. Kurshetsov, V. Obraztsov, V. Semenov, O. Yushchenko

Institute for High Energy Physics, 142281 Protvino (MO), Russia²⁰

G. D'Agostini

*Dipartimento di Fisica, Sapienza Università di Roma and
Sezione dell'INFN di Roma I, I-00185 Roma, Italy*

E. Leonardi, M. Serra, P. Valente

Sezione dell'INFN di Roma I, I-00185 Roma, Italy

A. Fucci, A. Salamon

Sezione dell'INFN di Roma Tor Vergata, I-00133 Roma, Italy

B. Bloch-Devaux²¹, B. Peyaud

DSM/IRFU – CEA Saclay, F-91191 Gif-sur-Yvette, France

J. Engelfried

Instituto de Física, Universidad Autónoma de San Luis Potosí, 78240 San Luis Potosí, Mexico²²

D. Coward

SLAC National Accelerator Laboratory, Stanford University, Menlo Park, CA 94025, USA

V. Kozhuharov²³, L. Litov

Faculty of Physics, University of Sofia, 1164 Sofia, Bulgaria²⁴

R. Arcidiacono²⁵, S. Bifani⁵

Dipartimento di Fisica dell'Università e Sezione dell'INFN di Torino, I-10125 Torino, Italy

C. Biino, G. Dellacasa, F. Marchetto

Sezione dell'INFN di Torino, I-10125 Torino, Italy

T. Numao, F. Retière

TRIUMF, Vancouver, British Columbia, V6T 2A3, Canada

*Corresponding author, email: nicolas.lurkin@cern.ch, michal.koval@cern.ch

†Deceased

¹Supported by a Royal Society University Research Fellowship

²Supported by ERC Starting Grant 336581

³Present address: CERN, CH-1211 Genève 23, Switzerland

⁴Present address: CIEMAT, E-28040 Madrid, Spain

⁵Present address: School of Physics and Astronomy, University of Birmingham, Birmingham, B15 2TT, UK

⁶Present address: Sezione dell'INFN di Perugia, I-06100 Perugia, Italy

⁷Present address: Ruprecht-Karls-Universität Heidelberg, D-69120 Heidelberg, Germany

⁸Present address: Institute of Nuclear Research and Nuclear Energy of Bulgarian Academy of Science (INRNE-BAS), Sofia, Bulgaria

⁹Funded by the National Science Foundation under award No. 0338597

¹⁰Also at Dipartimento di Fisica, Università di Modena e Reggio Emilia, I-41125 Modena, Italy

¹¹Also at Dipartimento di Fisica, Università di Firenze, I-50019 Sesto Fiorentino, Italy

¹²Also at Istituto di Fisica, Università di Urbino, I-61029 Urbino, Italy

¹³Present address: Università di Roma "La Sapienza, Roma, Italy

¹⁴Funded by the German Federal Minister for Education and Research (BMBF) under contract 05HA6UMA

¹⁵Present address: Physics Department, Imperial College London, London, SW7 2BW, UK

¹⁶Present address: Sezione dell'INFN di Pisa, I-56100 Pisa, Italy

¹⁷Present address: Dipartimento di Fisica dell'Università e Sezione dell'INFN di Padova, I-35131 Padova, Italy

¹⁸Present address: Dipartimento di Fisica dell'Università e Sezione dell'INFN di Pisa, I-56100 Pisa, Italy

¹⁹Present address: Department of Physics, University of Liverpool, Liverpool, L69 7ZE, UK

²⁰Partly funded by the Russian Foundation for Basic Research grant 12-02-91513

²¹Present address: Dipartimento di Fisica dell'Università di Torino, I-10125 Torino, Italy

²²Funded by Consejo Nacional de Ciencia y Tecnología (CONACyT) and Fondo de Apoyo a la Investigación (UASLP)

²³Also at Laboratori Nazionali di Frascati dell'INFN, Italy

²⁴Funded by the Bulgarian National Science Fund under contract DID02-22

²⁵Also at Università degli Studi del Piemonte Orientale, I-13100 Vercelli, Italy

Introduction

The Dalitz decay $\pi_D^0 \rightarrow e^+e^-\gamma$ with a branching fraction of $\mathcal{B} = (1.174 \pm 0.035)\%$ [1] proceeds through a $\pi^0 \rightarrow \gamma\gamma^*$ process with an off-shell photon converting into an e^+e^- pair. The π^0 electromagnetic transition form factor (TFF) describes the deviation of this transition from a point-like interaction. It is an input to the computation of the $\pi^0 \rightarrow e^+e^-$ decay rate [2], as well as the hadronic light-by-light scattering contribution to the muon anomalous magnetic moment $(g-2)_\mu$ which at present contributes the second largest uncertainty on its Standard Model value [3]. The commonly used kinematic variables are defined in terms of the e^\pm and π^0 four-momenta (p_{e^\pm}, p_{π^0}) as

$$x = \left(\frac{M_{ee}}{m_{\pi^0}}\right)^2 = \frac{(p_{e^+} + p_{e^-})^2}{m_{\pi^0}^2}, \quad y = \frac{2p_{\pi^0} \cdot (p_{e^+} - p_{e^-})}{m_{\pi^0}^2(1-x)},$$

with the allowed kinematic region defined as

$$r^2 = \left(\frac{2m_e}{m_{\pi^0}}\right)^2 \leq x \leq 1, \quad |y| \leq \sqrt{1 - \frac{r^2}{x}},$$

where m_e and m_{π^0} are the corresponding PDG [1] masses, and M_{ee} is the invariant mass of the e^+e^- pair. The differential decay width reads [4]

$$\frac{d^2\Gamma(\pi_D^0)}{dx dy} = \frac{\alpha}{4\pi} \Gamma(\pi_{2\gamma}^0) \frac{(1-x)^3}{x} \left(1 + y^2 + \frac{r^2}{x}\right) (1 + \delta(x, y)) |\mathcal{F}(x)|^2,$$

where $\Gamma(\pi_{2\gamma}^0)$ is the $\pi^0 \rightarrow \gamma\gamma$ decay width, the function $\delta(x, y)$ describes the radiative corrections and $\mathcal{F}(x)$ is the electromagnetic transition form factor of the π^0 to a real and virtual photon. The function $\mathcal{F}(x)$ is expected to vary slowly in the kinematic region of the π_D^0 decay and is usually approximated by a linear expansion $\mathcal{F}(x) = 1 + ax$, where a is the *slope* parameter. The vector meson dominance (VMD) model [5, 6] predicts a π^0 TFF slope value of $a \approx 0.03$, in agreement with further theoretical estimates [7–10].

The TFF slope has been determined in the time-like momentum transfer region by measuring the π_D^0 decay rate [11–15], all including radiative corrections. The TFF has been measured in the space-like momentum transfer region in the reaction $e^+e^- \rightarrow e^+e^-\pi^0$, where the π^0 is produced by the fusion of two photons radiated by the incoming beams and decays to two detected photons [16]. The current world average $a = 0.032 \pm 0.004$ [1] is obtained from time-like measurements [12–14] and the extrapolation of space-like data [16] using a VMD model.

The NA62 experiment at the CERN SPS collected in 2007 a large sample of charged kaons decaying in flight in vacuum with a minimum-bias trigger configuration [17]. The K^\pm decays represent a source of tagged neutral pions; the $K^\pm \rightarrow \pi^\pm\pi^0$ ($K_{2\pi}$) decay channel accounts for 63% of π^0 production. The mean free path of the neutral pion in the NA62 experimental conditions is negligible (few μm). This letter reports a model-independent measurement of the π^0 TFF slope parameter from an analysis of 1.11×10^6 $K_{2\pi}$ decays followed by the prompt π_D^0 decay (denoted $K_{2\pi D}$) using the full NA62 2007 data set.

1 Beam and detector

The NA62 experimental setup used in 2007 was composed of the NA48 detector [18] and a modified beam line [19] of the earlier NA48/2 experiment.

The beam line was designed to provide simultaneously K^+ and K^- beams. The primary 400 GeV/c proton beam delivered by the SPS impinged on a beryllium target of 40 cm length and 0.2 cm diameter. The secondary beam momenta were selected by magnets in a four dipole achromat and a momentum-defining slit incorporated into a beam dump. This 3.2 m thick copper/iron block provided the possibility to block either of the K^+ or K^- beams. The selected particles had a central momentum of 74 GeV/c with a spread of ± 1.4 GeV/c (rms). The beams

were focused and collimated before entering a 114 m long cylindrical vacuum tank containing the fiducial decay volume. The beams were mostly composed of π^\pm , with a K^\pm fraction of approximately 6%. Since the muon halo sweeping system was optimised for the positive beam in 2007, most of the data were recorded with the single K^+ beam to reduce the halo background. The K^+ and K^- beams were deflected horizontally by a steering magnet at the entrance of the fiducial decay volume at angles of $\pm(0.23 \text{ to } 0.30)$ mrad with respect to the detector axis, to compensate for the opposite ∓ 3.58 mrad deflection by the downstream spectrometer magnet. The polarities of those magnetic fields were regularly simultaneously reversed to reduce the effects caused by an asymmetry in the detector acceptance.

The momenta of charged particles were measured by a spectrometer composed of four drift chambers (DCH) and a dipole magnet placed between the second and third chamber providing a horizontal transverse momentum kick of $265 \text{ MeV}/c$ to singly-charged particles. The measured momentum resolution was $\sigma_p/p = 0.48\% \oplus 0.009\% \cdot p$, where the momentum p is expressed in GeV/c . The spectrometer was housed in a tank filled with helium at nearly atmospheric pressure, separated from the decay volume by a thin ($3 \times 10^{-3} X_0$) KevlarTM window.

The photons were detected and measured by a liquid krypton (LKr) electromagnetic calorimeter, which is a quasi-homogeneous ionisation chamber with an active volume of 6.7 m^3 of octagonal cross-section and a thickness of 127 cm, corresponding to $27 X_0$. The LKr volume is divided into 13,248 cells of about $2 \times 2 \text{ cm}^2$ cross section without longitudinal segmentation. The measured energy resolution was $\sigma_E/E = 3.2\%/\sqrt{E} \oplus 9\%/E \oplus 0.42\%$, and the spatial resolution for the transverse coordinates x and y was $0.42 \text{ cm}/\sqrt{E} \oplus 0.06 \text{ cm}$, where the energy is given in GeV in both cases.

A scintillator hodoscope (HOD) was located between the spectrometer and the LKr calorimeter. It consists of a set of scintillators arranged into a plane of 64 vertical counters followed by a plane of 64 horizontal counters. Each plane was divided into four quadrants of 16 counters providing a fast trigger signal for charged particles.

2 Data sample and trigger logic

The analysis is based on the full data set collected during 4 months in 2007, corresponding to about 2×10^{10} K^\pm decays in the vacuum tank. A total of 65% (8%) of the K^+ (K^-) flux was collected in single-beam mode while the remaining 27% were collected with simultaneous K^\pm beams with a K^+/K^- flux ratio of 2.0. During part of the data taking (55% of the K^\pm flux), a $9.2 X_0$ thick transverse horizontal electron absorber lead (Pb) bar was installed between the two HOD planes, approximately 1.2 m in front of the LKr calorimeter, to study muon-induced electromagnetic showers [17]. A total of 11 rows of LKr calorimeter cells were shadowed by the bar, corresponding to about 10% of the total number of cells.

The 100 kHz kaon decay rate in the vacuum volume during the spill enabled the use of a minimum-bias trigger configuration with a highly efficient trigger chain optimised to select events with at least one electron (e^\pm) track.

The low level hardware trigger required a coincidence of hits in at least one hodoscope quadrant in both planes (the Q_1 condition), upper and lower cuts on the hit multiplicity in the drift chambers (the 1-track condition), and a minimum total energy deposit of 10 GeV in the LKr calorimeter (the E_{LKr} condition). The high level software trigger (HLT) condition required at least one track with $5 \text{ GeV}/c < p < 90 \text{ GeV}/c$ and $E/p > 0.6$, where E is the energy reconstructed in the calorimeter and p is the momentum reconstructed in the spectrometer. Downscaled minimum bias trigger streams were collected to evaluate the trigger efficiencies.

3 Simulated samples and π_D^0 decay simulation

Monte Carlo (MC) simulations of the $K_{2\pi D}$ decay chain and two other K^\pm decay chains producing π^0 Dalitz decays, $K^\pm \rightarrow \pi_D^0 e^\pm \nu$ and $K^\pm \rightarrow \pi_D^0 \mu^\pm \nu$ (denoted K_{e3D} and $K_{\mu3D}$, respectively),

were performed with a π^0 TFF slope $a_{\text{MC}} = 3.2 \times 10^{-2}$. Separate simulated samples, proportionally to the number of kaon decays recorded, were produced for each data taking condition. The total simulated sample amounts to 386 M $K_{2\pi D}$, 105 M $K_{\mu 3D}$ and 103 M $K_{e 3D}$ events within the 97 m long fiducial decay region. All these modes contribute to the π_D^0 sample, although the selection is optimized for $K_{2\pi D}$.

The radiative corrections to the total [4] and differential [20–22] π_D^0 decay widths have been studied extensively. They have to be considered for the TFF measurement since their effect on the x spectrum is comparable to the effect of the TFF. The calculation of the radiative corrections [22] implemented in the MC simulation of the π_D^0 decay for the present analysis includes real photon emission from the π_D^0 decay vertex. It also includes the one-photon irreducible contribution, neglected in earlier studies, which has an effect of $|\Delta a| \approx 0.5 \times 10^{-2}$ on the slope of the x spectrum. Higher order correction terms not included in the simulation contribute to the slope by $|\Delta a| < 0.01 \times 10^{-2}$, which is considered as a systematic uncertainty (Table 1).

4 Data analysis

4.1 Event reconstruction and selection

Hits and drift times in the DCH and a detailed map of the magnetic field are used to reconstruct track directions and momenta. Three-track vertices are reconstructed by a Kalman filter algorithm extrapolating track segments from the upstream part of the spectrometer into the decay volume, taking into account multiple scattering in the helium and the Kevlar window, the Earth’s magnetic field and residual vacuum tank magnetization. The reconstructed $K^\pm \rightarrow \pi^\pm \pi^+ \pi^-$ invariant mass and the missing mass in the $K^\pm \rightarrow \mu^\pm \nu$ decay are monitored and used for fine calibration of the spectrometer momentum scale and DCH alignment. Clusters of energy deposition in the LKr calorimeter are found by locating maxima in space and time in the digitized pulses from individual cells. Reconstructed energies are corrected for energy outside the cluster boundaries, energy lost in isolated inactive cells (0.8% of the total number), sharing of energy between clusters, and non-linearity for clusters with energy below 11 GeV. Electrons produced in $K^\pm \rightarrow \pi^0 e^\pm \nu$ decays are used to calibrate the energy response.

The main $K_{2\pi D}$ selection criteria are the following.

- The event should contain exactly one reconstructed 3-track vertex, which should be located within the fiducial decay region and be geometrically compatible with a beam kaon decay. The vertex charge q_{vtx} , defined as the sum of the track charges, should match the beam charge in the single-beam mode. Otherwise it should satisfy a relaxed condition $|q_{\text{vtx}}| = 1$. The track with the charge opposite to q_{vtx} is necessarily an e^\pm candidate, while the same-sign tracks can be either π^\pm or e^\pm candidates.
- The tracks are required to be in time (within 25 ns of the trigger time and 15 ns of each other), and within the geometrical acceptance of the drift chambers. The allowed track momentum range is (2–74) GeV/ c , excluding the low momentum range where a 2% deficit of data with respect to MC simulation is seen. Events with a photon converting into an e^+e^- pair in the material in or in front of DCH1 (Kevlar window, helium) are suppressed by requiring a minimum distance of 2 cm between the impact points of every track pair in the first drift chamber, as verified by simulation of $K_{2\pi}$ decays.
- Reconstructed clusters of energy deposition in the LKr calorimeter are used to identify photon candidates. A photon candidate cluster should be geometrically isolated from the track impact points in the LKr calorimeter ($d_t > 20$ cm from the same-sign tracks and $d_t > 10$ cm from the remaining track), within 10 ns of each track and with more than 2 GeV of energy. The photon 4-momentum is reconstructed assuming that the photon originates from the same vertex as the tracks. If more than one photon candidate is found, the event is rejected.

- The total reconstructed momentum should be compatible with the beam momentum, in the range (70–78) GeV/ c , and there should be no missing transverse momentum with respect to the beam axis within the resolution: $p_t^2 < 10^{-5} (\text{GeV}/c)^2$. Particle identification using an E/p ratio is not required thanks to the low background in the sample, reducing the systematics associated to the misidentification and increasing the $K_{2\pi D}$ acceptance by more than a factor of two. The π/e ambiguity for the two same-sign tracks is resolved by testing the two possible mass assignments. For each hypothesis, the reconstructed kinematic variables should be $|x|, |y| < 1$, and the reconstructed $e^+e^-\gamma$ and $\pi^\pm\pi^0$ masses should be close to the nominal ones: $M_{ee\gamma}$ in the range (115–145) MeV/ c^2 and $M_{\pi\pi}$ in the range (460–520) MeV/ c^2 . Only events with a single valid hypothesis are selected. The probability of correct (incorrect) mass assignment evaluated with the $K_{2\pi D}$ MC sample is 99.62% (0.02%). The remaining 0.36% of events have either zero or two valid hypotheses and are rejected.
- The trigger conditions described in Section 2 are reproduced on simulated samples. To eliminate edge effects due to different calibration and resolution between the trigger and the offline analysis, tighter variants of the trigger criteria are applied to both data and MC samples. The offline E_{LKr} condition requires a minimum of 14 GeV of electromagnetic energy in the LKr calorimeter summed over the reconstructed photon and e^\pm clusters. The offline condition corresponding to the HLT requires at least one track whose impact point on the LKr calorimeter front plane is within its acceptance and not behind the Pb bar, $p > 5.5 \text{ GeV}/c$ and $E/p > 0.8$, effectively requesting that at least one e^\pm track is detected in the calorimeter.
- A 1% deficit in the data/MC ratio is seen for events with $x < 0.01$ due to the steeply falling acceptance. For this reason the signal region is defined as $x > 0.01$, equivalent to $M_{ee} > 13.5 \text{ MeV}/c^2$.

The selected $K_{2\pi D}$ sample amounts to 1.11×10^6 events. The overall acceptances of the selection evaluated with MC simulations are 1.90% for $K_{2\pi D}$ decays, 0.02% for $K_{\mu 3D}$ decays and 0.01% for $K_{e 3D}$ decays. The $K_{2\pi D}$ acceptances for periods with and without the Pb bar installed are 1.64% and 2.23%, respectively.

The reconstructed $\pi^\pm\pi^0$ and $e^+e^-\gamma$ invariant mass spectra are shown in Fig. 1; the mass resolutions obtained from a Gaussian fit are 3.7 MeV/ c^2 and 1.5 MeV/ c^2 (rms), respectively. The reconstructed spectrum of the x variable and the acceptances for the decay channels considered are shown in Fig. 2. The e^+e^- mass resolution determined from the $K_{2\pi D}$ MC sample can be approximated by $\sigma_{ee} = 0.9\% \cdot M_{ee}$, which translates into the resolution on the x variable as $\sigma_x = 1.8\% \cdot x$.

4.2 Fit procedure

A χ^2 fit with free MC normalisation in equally populated bins comparing the data and MC reconstructed x distributions is performed to extract the TFF slope. A number of slope hypotheses a_h are tested by reweighting a single set of MC events simulated with a slope $a_{\text{MC}} = 3.2 \times 10^{-2}$ using the weights

$$w(a_h) = \frac{(1 + a_h x_{\text{MC}})^2}{(1 + a_{\text{MC}} x_{\text{MC}})^2},$$

where x_{MC} is the true x value for each event. The minimization of the χ^2 test statistics yields the following result:

$$a = (3.68 \pm 0.48 \pm 0.18) \times 10^{-2},$$

where the uncertainties are statistical due to the limited data and MC sample sizes. The fit gives $\chi^2/\text{ndf} = 54.8/49$, which has a p -value of 26.4%. The fit result is illustrated in Fig. 3.

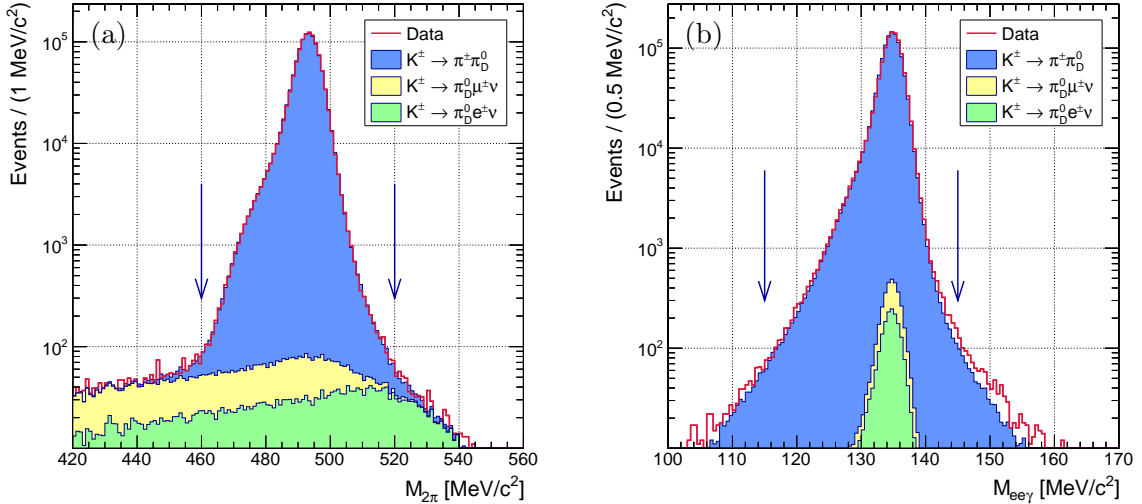


Figure 1: Reconstructed (a) $\pi^{\pm}\pi^0$ and (b) $e^+e^-\gamma$ mass distributions for data and simulated components. The radiative shoulders in the reconstructed masses are well reproduced in the MC thanks to the simulation of the radiative photon. The adopted mass selection criteria represented by the arrows are asymmetric with respect to the nominal K^{\pm} and π^0 masses.

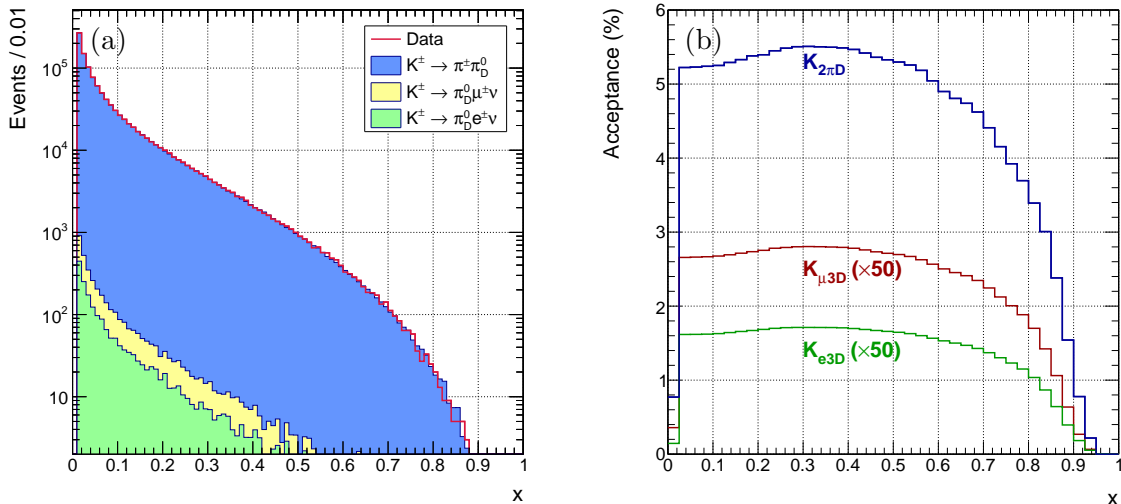


Figure 2: (a) Spectra of the reconstructed x variable for data and MC components. (b) Acceptances of the $K_{2\pi D}$ selection for each decay as functions of the x variable. The acceptances for $K_{\ell 3D}$ decays ($\ell = e; \mu$) are scaled up by a factor of 50. The drop in the first bin is due to the signal region definition ($x > 0.01$).

Using a quadratic function $|\mathcal{F}(x)|^2 = 1 + 2bx + cx^2$, the fit results are $b = (3.71 \pm 0.51) \times 10^{-2}$ and $c = 0.00 \pm 0.19$.

4.3 Systematic effects

4.3.1 Calibration, resolution and beam simulation

The spectrometer momentum scale modifies proportionally the x variable. The corrections applied to the momentum calibration have a typical relative size of the order of 10^{-3} . The sensitivity of the fit to a residual miscalibration has been assessed conservatively by turning the corrections off, leading to a shift of the fit result of $\Delta a = -0.16 \times 10^{-2}$ considered as the

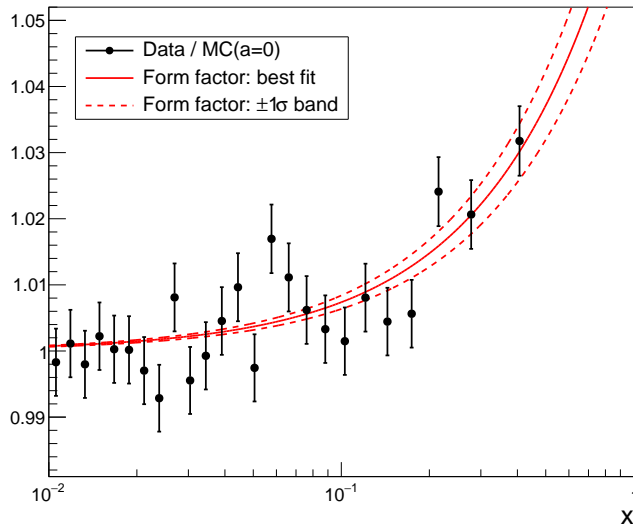


Figure 3: Ratio of the reconstructed x distributions for data and MC, where the MC sample corresponds to $a = 0$. The effect of a positive TFF slope ($a > 0$) is clearly seen in this illustration. Data and MC events are distributed into 25 equally populated bins; the horizontal positions of the markers correspond to the bin barycentres. The solid line represents $|\mathcal{F}(x)|^2$ with the measured central slope value: $a = 3.68 \times 10^{-2}$. The dashed lines indicate the $\pm 1\sigma$ band. Only the statistical uncertainties are shown.

systematic uncertainty on the spectrometer calibration. A similar procedure is applied for the chamber misalignment correction with no significant effect on the fit result.

The spectrometer mass resolution has been evaluated separately for individual data-taking periods using samples of $K^\pm \rightarrow \pi^\pm \pi^+ \pi^-$ decays. The maximum relative difference observed on the resolution of the reconstructed squared 3-pions mass between data and MC is 2%. Scaling the MC resolution of the x variable by 0.98 results in a shift of $\Delta a = 0.05 \times 10^{-2}$, which is considered as a systematic uncertainty.

The corrections applied to the energies measured in the LKr calorimeter affect the TFF slope result indirectly through the photon selection acceptance. A correction for the non-linearity in the energy response in the data sample with an alternative function is used to evaluate the sensitivity to the correction function, resulting in a shift of $\Delta a = 0.03 \times 10^{-2}$. A global photon energy scaling factor of 1.001, which is the typical size of the energy corrections, applied only in the MC sample causes a shift of $\Delta a = 0.02 \times 10^{-2}$. The overall systematic uncertainty due to the LKr energy calibration is assigned as the sum of these two effects in quadrature: $\Delta a = 0.04 \times 10^{-2}$.

The beam momentum is simulated according to the central value measured separately for different data taking periods from fully reconstructed $K^\pm \rightarrow \pi^\pm \pi^+ \pi^-$ decays. A remaining discrepancy between data and MC in the tails of the beam momentum spectrum affects the TFF slope measurement through the K^\pm momentum dependence of the acceptance. After applying a correction to improve the spectrum data/MC agreement, the measured slope shifts by $\Delta a = 0.03 \times 10^{-2}$, which is considered as a systematic uncertainty.

4.3.2 Trigger efficiency

The efficiencies of individual components of the signal trigger chain have been measured using control data samples collected via alternative trigger chains. Since no inefficient events have been found, upper limits on the inefficiencies at 90% CL have been evaluated for each trigger conditions: 0.06% (Q_1), 0.10% (1-track), 0.03% (E_{LKr}) and 0.03% (HLT).

Possible systematic effects caused by each trigger condition have been investigated separately by removing potentially inefficient events either from the data or the MC sample. The Q_1

efficiency is modeled by introducing fully inefficient gaps between the HOD quadrants with 0.2 mm width tuned using data/MC comparison in other decay channels. This leads to a Q_1 inefficiency of 0.02% for $K_{2\pi D}$ events. Energetic photons may initiate showers by interacting with the beam pipe material, causing the DCH hit multiplicities to exceed the limits allowed by the 1-track trigger condition. The sensitivity to this effect is tested by removing from the MC $K_{2\pi D}$ sample 0.10% of events with a radiative photon with an energy above 0.5 GeV traversing the beam pipe. For the E_{LKr} and HLT triggers, events closest to failing a trigger condition are removed from the data sample. Those are events with the lowest reconstructed energy in the LKr calorimeter for the E_{LKr} condition, and events with the lowest maximum track E/p ratio for the HLT condition. In both cases the fraction of removed events is equal to the upper limits on inefficiencies quoted above. The only sizeable change in the TFF slope result has been observed by testing the E_{LKr} trigger condition, resulting in a systematic uncertainty estimate of $\Delta a = 0.06 \times 10^{-2}$.

4.3.3 Backgrounds

The effect of accidental background is investigated by releasing independently the timing cuts and constraints on the numbers of tracks and vertices in the selection. The number of additional events included into the data sample for each variation of the selection is less than 6×10^3 . The total systematic uncertainty due to accidentals is evaluated to be $\Delta a = 0.15 \times 10^{-2}$.

The misidentification of charged particles is studied by a modification of the selection criteria. The pion mass is assigned to the track with the charge opposite to q_{vtx} in the kinematic event identification to select $K^\pm \rightarrow e^\pm e^\pm \pi^\mp \gamma$ candidates. Since this process violates lepton number conservation, all events passing this ‘‘LNV selection’’ are considered to be events with misidentified tracks. A total of 188 events from the full data set pass the LNV selection. Using the same selection on the MC samples, it is estimated that most of those events are genuine $K_{2\pi D}$ decays with misidentified π^\pm and e^\mp tracks, while 42 ± 18 data events are not accounted for. The x distribution of these events is added to the reconstructed $K_{2\pi D}$ MC one. The TFF slope shifts by $\Delta a = 0.06 \times 10^{-2}$, which is considered as a systematic uncertainty.

Removing the $K_{\mu 3 D}$ and $K_{e 3 D}$ MC samples from the fit procedure results in a shift of the slope of $\Delta a = 0.01 \times 10^{-2}$. This is considered as an estimate of the systematic uncertainty on the TFF slope due to the neglected π^0 sources as the other neglected kaon decay modes producing neutral pions account for less than 4% of π^0 production.

The acceptance of the $K_{2\pi D}$ selection for the $K_{2\pi}$ decay followed by $\pi^0 \rightarrow \gamma\gamma$ is estimated with MC simulations to be smaller than 10^{-7} , confirming that the minimal distance requirement between tracks in the first DCH efficiently removes the events with photon conversion. The reduction of detector acceptance by the Pb bar (Section 2) does not lead to any systematic uncertainties since events with a particle within the lead bar acceptance are discarded.

5 Result

The statistical and systematic uncertainties discussed in the previous sections are summarised in Table 1. The result of the measurement of the π^0 TFF slope parameter is

$$a = (3.68 \pm 0.51_{\text{stat}} \pm 0.25_{\text{syst}}) \times 10^{-2} = (3.68 \pm 0.57) \times 10^{-2},$$

which is in good agreement with the theoretical predictions [5–10]. A comparison with previous π_D^0 measurements is shown in Fig. 4.

Table 1: Summary of the uncertainties.

Source	$\Delta a \times 10^2$
Statistical – data	0.48
Statistical – MC	0.18
Total statistical	0.51
Spectrometer momentum scale	0.16
Spectrometer resolution	0.05
LKr calibration	0.04
Beam momentum spectrum simulation	0.03
Calorimeter trigger inefficiency	0.06
Accidental background	0.15
Particle misidentification	0.06
Neglected π_D^0 sources	0.01
Higher order radiative contributions	< 0.01
Total systematic	0.25

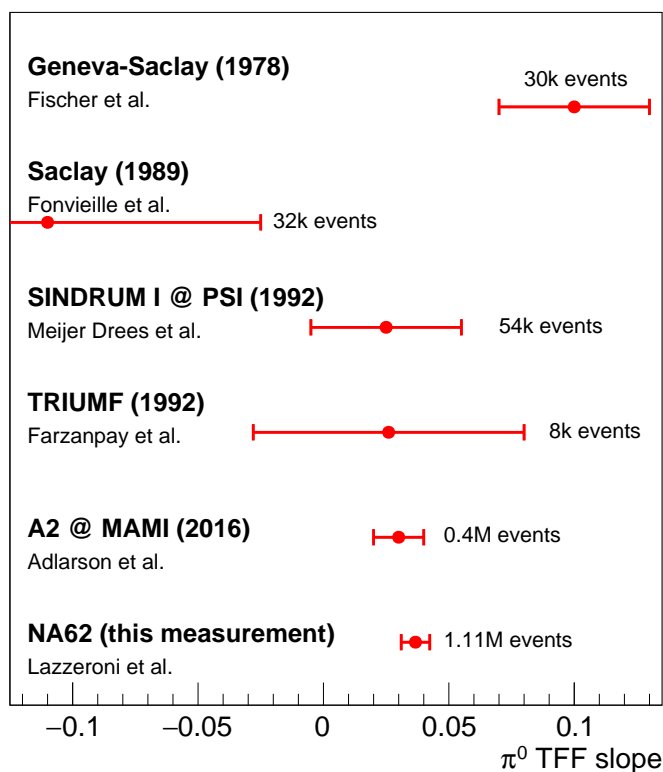


Figure 4: Comparison of the π^0 TFF slope measurements in the time-like momentum transfer region [11–15].

Conclusions

The slope of the electromagnetic transition form factor of the π^0 is measured from a sample of 1.11×10^6 π^0 Dalitz decays. The result $a = (3.68 \pm 0.57) \times 10^{-2}$ represents the most precise measurement of the form factor slope in the time-like momentum region. The 15% relative uncertainty represents an improvement by a factor of 2 with respect to the previous best measurement [15].

Acknowledgements

We express our gratitude to the staff of the CERN laboratory and the technical staff of the participating laboratories and universities for their efforts in the operation of the SPS accelerator, the experiment and data processing. We thank T. Husek for fruitful discussions and collaboration on the π_D^0 decay generator development.

References

- [1] C. Patrignani *et al.*, *Chin. Phys. C* **40**, 100001 (2016).
- [2] T. Husek, K. Kampf, and J. Novotný, *Eur. Phys. J. C* **74**, 3010 (2014).
- [3] A. Nyffeler, *Phys. Rev. D* **94**, 053006 (2016).
- [4] D. W. Joseph, *Il Nuovo Cimento* **16**, 997 (1960).
- [5] M. Gell-Mann and F. Zachariasen, *Phys. Rev.* **124**, 953 (1961).
- [6] P. Lichard, *Phys. Rev. D* **83**, 037503 (2011).
- [7] K. Kampf, M. Knecht, and J. Novotný, *Eur. Phys. J. C* **46**, 191 (2006).
- [8] P. Masjuan, *Phys. Rev. D* **86**, 094021 (2012).
- [9] M. Hoferichter, B. Kubis, S. Leupold, F. Niecknig, and S. P. Schneider, *Eur. Phys. J. C* **74**, 3180 (2014).
- [10] T. Husek and S. Leupold, *Eur. Phys. J. C* **75**, 586 (2015).
- [11] J. Fischer *et al.*, *Phys. Lett. B* **73**, 359 (1978).
- [12] H. Fonvieille *et al.*, *Phys. Lett. B* **233**, 65 (1989).
- [13] F. Farzanpay *et al.*, *Phys. Lett. B* **278**, 413 (1992).
- [14] R. Meijer Drees *et al.*, *Phys. Rev. D* **45**, 1439 (1992).
- [15] P. Adlarson *et al.*, arXiv:1611.04739 [hep-ex] (2016).
- [16] H. J. Behrend *et al.*, *Z. Phys. C* **49**, 401 (1991).
- [17] C. Lazzeroni *et al.*, *Phys. Lett. B* **719**, 326 (2013).
- [18] V. Fanti *et al.*, *Nucl. Instrum. Meth. A* **574**, 433 (2007).
- [19] J. R. Batley *et al.*, *Eur. Phys. J. C* **52**, 875 (2007).
- [20] B. E. Lautrup and J. Smith, *Phys. Rev. D* **3**, 1122 (1971).
- [21] K. O. Mikaelian and J. Smith, *Phys. Rev. D* **5**, 1763 (1972).
- [22] T. Husek, K. Kampf, and J. Novotný, *Phys. Rev. D* **92**, 054027 (2015).